Supplementary Material

New insights on Anthropocene fire management from pre-Columbian Amazonian Dark Earth forests

S. Yoshi Maezumi[1*], Mark Robinson[1], Jonas Gregorio de Souza[1], Dunia Urrego[2], Denise Schaan[3], Daiana Alves[1], Jose Iriarte[1]

[1]*Department of Archaeology, College of Humanities, University of Exeter, Laver Building, North Park Road, Exeter EX4 4QE, UK*

[2]*Department of Geography, College of Life and Environmental Sciences, University of Exeter, Amory Building, Rennes Drive. Exeter, EX4 4RJ, UK*

[3]*Department of Anthropology, Federal University of Pará, Belém 66075-110, Brazil*

*** Correspondence:** S. Yoshi Maezumi: s.y.maezumi@exeter.ac.uk

1 Supplementary Data

1.1 Supplementary Methods (M_x)

M1 Paleoecological age-depth model.

The chronology for the LC sediment core relies on six radiocarbon (^{14}C) dates, ^{210}Pb radionuclide analysis of recent sedimentation and an age-depth model constructed in Bacon v2.2 (Blaauw et al., 2007) within R (R Foundation for Statistical Computing, 2014). Ages for the upper sediments of core LC were modelled using ^{210}Pb radionuclide analyses following standard procedures (Appleby, 2001). Atmospheric fallout of ^{210}Pb can be used to estimate the age of sedimentary sequences by measuring the rate of its decay across approximately six to nine half-lives, or 130 to 200 years. The addition of ^{210}Pb dating was used in this study to develop a robust chronology for the most recent paleoenvironmental changes, which also to provides an important validation tool for the youngest part of the age-depth model that otherwise relies on radiocarbon analyses. Radiocarbon ages that are younger than ~250 cal yrs B.P. contain large calibration uncertainties due to a ~200 year plateau in the calibration curve and are of limited use for tightly constraining recent centuries when developing an age-depth model . Activity of ^{210}Pb was determined by measuring alpha decay of its daughter product ^{210}Po as a proxy (Flynn, 1968). Sediment subsample was spiked with a ^{209}Po chemical yield tracer, acid digested using sequential HNO_3:H_2O_2:HCl (1:2:1) chemical washes at 90°C, and then extracted from the solution, electroplated onto a silver disc, and measured using an Ortec Octête Plus Integrated Alpha-Spectrometry System at the University of Exeter. The age-depth profile was calculated from the total ^{210}Pb inventory, the ^{210}Pb decay constant (0.03114 yr^{-1}), sample-specific activity and cumulative mass using the constant rate of supply model (Appleby, 2001), which provided ten ages for the top 0.17 m of the core with modelled root-mean-square-error 2σ uncertainties. Bulk sediment organic material was collected from the sediment core for conventional AMS radiocarbon dating (Stuiver and Polach, 1977) and

sent to Beta Analytic for standard pretreatments and radiocarbon analysis. Radiocarbon ages were calibrated within Bacon using IntCal13 (Reimer et al., 2013) and modelled using Student-t test distributions with wide tails to negate the need of identifying and removing potential outliers in the age-depth model (Andrés and Pérez, 2009; Blaauw and Christen, 2011). The use of Bacon and Bayesian statistics to reconstruct the accumulation history at LC allowed us to include every radiocarbon date that was taken throughout the LC core and develop robust estimations of age-depth uncertainty. Age-depth model mean accumulation rate priors in Bacon were calculated using the ^{14}C chronology (*acc.mean=42*) and memory priors were set slightly below default so that the model would capture accumulation rate changes driven by variable sediment delivery from the catchment (*mem.strength=2; mem.mean=0.4*). Model means and 2 σ age distributions were calculated from millions of Markov chain Monte Carlo age-depth iterations through the core. The distribution of profile iterations identified radiocarbon ages Beta-469035 and Beta-469038 as potential outliers. Rather than omit these data points, they were retained and contributed to the uncertainty distribution of the model. For example, at depths 1.00 ±0.005 m and 1.15 ±0.005 m where a possible reversal occurs, the outliers allow for a greater range of age-depth iterations, which provide age estimations (3562 ±423 and 4555 ±514 cal yr B.P. respectively) with larger uncertainties in comparison to the younger part of the model where the age profile distributions were narrower and showed more certainty.

M2 Magnetic susceptibility.

Magnetic susceptibility (MS) was measured to identify mineralogical variation in the sediments (Nowaczyk, 2001). The MS of sediments is reflective of the relative concentration of ferromagnetic (high positive MS), paramagnetic (low positive MS), and diamagnetic (weak negative MS) minerals or materials. Typically, sediment derived from freshly eroded rock has a relatively high MS, whereas sediments that are dominated by organic debris, evaporites, or sediments that have undergone significant diagenetic alteration have a low or even negative MS (Reynolds et al., 2001). Shifts in the magnetic signature of the sediment can be diagnostic of a disturbance event (Gedye et al., 2000).

M3 X-ray fluorescence.

X-ray fluorescence (XRF) analysis was conducted using a portable XRF Thermo Scientific Niton 3L3t GOLDD at the University of Reading at a step size of 2000 or 5000 µm. A micro-X-ray beam focused through a flat capillary waveguide was used to irradiate samples to enable both X-radiography and XRF analysis. Data were acquired incrementally at 0.25 cm contiguous intervals by advancing the split core through the X-ray beam (Croudace et al., 2006) and results were normalized using z-scores.

M4 Loss-on-ignition.

Organic and carbonate sediment composition was determined by loss-on-ignition (LOI) conducted at 4 cm intervals throughout the core. For each sample, 1 cm^3 of sediment was dried in an oven at 100˚C for 24 hours. The samples underwent a series of 2 hour burns in a muffle furnace at 550˚C and 1000˚C to determine the relative percentage of the sample composed of organics and

carbonates. Concentration was determined by weight following standard methodology (Dean Jr, 1974).

M5 Pollen Analysis

In addition to the standard pollen digestion protocol, an additional sieving stage to concentrate large cultigen pollen types such as *Z. mays* (Whitney et al., 2012) was added. Equal numbers of exotic *Lycopodium clavatum* L. tablets (Stockmarr, 1971) were added to both the filtrate and residue of the sieved samples allow for direct comparison of cultigen pollen abundance with the standard terrestrial pollen counts (Whitney et al., 2012). Large pollen grains (>53 μm) concentrated through the fine-sieving methodology were scanned for *Z. mays* and other crop taxa producing large pollen such as *Manihot esculenta* and *Ipomoea batatas* (Whitney et al., 2012). The coarse fractions were counted to a standardized equivalent count of 2,000 *Lycopodium* grains (~ 3 to 4 slides). The pollen in the fine fractions was counted to the standard 300 terrestrial grains. *Mauritia/Mauritiella* were counted and totaled separately due to high concentrations. Larger non-crop pollen that was sieved into the coarse fraction (e.g. *Mauritia/Mauritiella*), was factored back into the total terrestrial pollen sums using abundance calculations from *Lycopodium* counts from the fine and coarse fractions using standard methods (Whitney et al., 2012). Where possible, members of the Moraceae family were identified to genus level using published pollen reference material and morphological descriptions (Burn and Mayle, 2008). Additionally, pollen taxa were grouped into edible trees, palms, and herbs, crops, other trees and herbs in the pollen diagram based on modern botanical classifications (Clement, 1999; Hanelt et al., 2001; Levis et al., 2017; Maezumi et al., 2018). In addition to edible palms (e.g. Mauritia/Mauritiella), we have included in the 'edible' category of all the plant taxa identified to the genus level in the pollen record that are ethnographically used as food resources in the Americas (Hanelt et al., 2001) after Maezumi et al. (2018). Over seventy percent of these pollen taxa are present in the modern botanical inventories, thus these pollen genera likely represent edible species in past anthropogenic forests around Lake Caranã. This edible plant classification is a conservative estimate since a large proportion of the families in the 'Other Trees and Herbs' category contain species that are edible, however, these taxa were excluded if they could not be taxonomically identified higher than family level.

M6 Local and Regional Macrocharcoal.

The LC sediment core was subsampled for macroscopic charcoal analysis at 0.5 cm intervals from 0 to 210 cm depth. Subsampled material (1 cm^3) was treated using standard protocol for charcoal pieces greater than 125 μm using a modified macroscopic sieving method (Brown and Power, 2013; Whitlock and Larsen, 2002). Charcoal counts were converted to charcoal influx (number of charcoal particles cm^{-2} yr^{-1}) and charcoal accumulation rates by dividing by the deposition time (yr cm^{-1}). Charcoal influx data (particles cm^{-2} yr^{-1}) were used as an indicator of *fire severity* (the amount of biomass consumed during a fire episode or period of increased burning). A regime shift detection algorithm (RSI) based on sequential t-tests was applied to determine the occurrence of statistically significant shifts in the charcoal influx data and plotted against charcoal influx data to identify significant changes in past fire regimes, interpreted here as indicators of changes in paleofire severity. CHAR statistical software (Higuera et al., 2009) was used to decompose charcoal data to identify distinct charcoal peaks based on a standard set of threshold criteria. The background component reflected the low-frequency portion of the CHAR series that varied in response to changes in the rate of total charcoal production and secondary charcoal transport (Higuera et al., 2007). Background charcoal is modeled using a curve-fitting algorithm (Higuera et al., 2010). If charcoal influxes exceed the background threshold, they are considered a peak. Charcoal peaks are

interpreted as a *fire episode* (a period of increased burning) because they cannot unambiguously be related to a single event (Brown and Power, 2013). The time difference between peaks is reflected in the fire return interval (*fire frequency*) for every 800 years. Estimates of fire frequency are obtained by summing and smoothing the peak series over a specified window width (Higuera et al., 2010).

Charcoal records are compiled from the Global Charcoal Database (GCD version 2.0) and analyzed using the paleofire R package software (version 1.1.8) (Blarquez et al., 2014). Eleven charcoal records between -3ºS and 0.2ºN and 43ºW to 54ºW that have greater than 20 charcoal samples are included in this analysis to create an RCC (Table 2, Figure 1). The sites from the eastern Amazon are selected to provide an average of regional biomass burning during the Holocene. To facilitate inter-site comparison, the eleven records are pretreated using standard protocol (Marlon et al., 2008; Power et al., 2008) for transforming and standardizing of individual records that includes: (1) transforming non-influx data (e.g. concentration particles cm^{-3}) to influx values (particle cm^{-2} yr^{-1}), (2) homogenizing the variance using the Box-Cox transformation, (3) rescaling the values using a minimax transformation to allow comparisons among sites, and (4) rescaling the values to z-scores using a base period of 200 years. Sites are smoothed with a 400-year half width smoothing window and a bootstrap of 100 years (Blarquez et al., 2014).

M7 SPD and site frequencies.

SPDs were built in OxCal using the Sum function and the IntCal13 calibration curve (Hogg et al., 2013; Ramsey and Lee, 2013) with an original dataset of 85 radiocarbon dates from the Lower Tapajós. In order to account for oversampling of some sites and phases within those sites, we applied a binning procedure (Goldberg et al., 2016; Shennan et al., 2013; Timpson et al., 2014). Dates within sites were ordered and those occurring within 100 years of each other were grouped into bins and merged with the R_combine function. Timpson et al. (Timpson et al., 2014) found that different values for the bin-width did not affect the final shape of the SPD. This procedure is necessary because a sum of the calibrated dates assumes that observations are independent, whereas this is not the case when multiple dates were obtained for single sites or phases within them, as was the case with many sites of the Tapajós. The final filtered dataset contained 52 dates. Despite the decrease in sample size, the filtered SPD is highly correlated with an SPD built with all radiocarbon dates ($r2 = 0.991$, $p < 0.001$).

References

Andrés, C. J., and Pérez, S. E. (2009). A new robust statistical model for radiocarbon data. *Radiocarbon* 51, 1047–1059. doi:DOI: 10.1017/S003382220003410X.

Appleby, P. G. (2001). "Chronostratigraphic techniques in recent sediments," in *Tracking environmental change using lake sediments. Volume 1: Basin analysis, coring and chronological techniques*, eds. W. M. Last and J. P. Smol (Dordrecht, Netherlands: Kluwer Academic Publishers).

Blaauw, M., and Christen, J. A. (2011). Flexible palaeoclimate age-depth models using an autoregresive gamma process. *Bayesian Anal.* 6, 457–474.

Blaauw, M., Christen, J. A., Mauquoy, D., van der Plicht, J., and Bennett, K. D. (2007). Testing the timing of radiocarbon-dated events between proxy archives. *The Holocene* 17, 283–288.

Blarquez, O., Vannière, B., Marlon, J. R., Daniau, A.-L., Power, M. J., Brewer, S., et al. (2014). Paleofire: An R package to analyse sedimentary charcoal records from the Global Charcoal Database to reconstruct past biomass burning. *Comput. Geosci.* 72, 255–261.

Brown, K. J., and Power, M. J. (2013). "Charred particle analyses.," in *The Encyclopedia of Quaternary Science* (Amsterdam, The Netherlands: Elsevier), 716–729.

Burn, M. J., and Mayle, F. E. (2008). Palynological differentiation between genera of the Moraceae family and implications for Amazonian palaeoecology. *Rev. Palaeobot. Palynol.* 149, 187–201. doi:10.1016/j.revpalbo.2007.12.003.

Clement, C. R. (1999). 1492 and the loss of Amazonian crop genetic resources. II. crop biogeography at contact. *Econ. Bot.* 53, 203–216. Available at: http://www.jstor.org/stable/4256180.

Croudace, I. W., Rindby, A., and Rothwell, R. G. (2006). ITRAX: description and evaluation of a new multi-function X-ray core scanner. *Spec. Publ. Soc. London* 267, 51.

Dean Jr, W. E. (1974). Determination of carbonate and organic matter in calcareous sediments and sedimentary rocks by loss on ignition: Comparison with other methods. *J. Sediment. Res.* 44, 242–248.

Flynn, W. W. (1968). The determination of low levels of polonium-210 in environmental materials. *Anal. Chim. Acta* 43, 221–227. doi:https://doi.org/10.1016/S0003-2670(00)89210-7.

Gedye, S. J., Jones, R. T., Tinner, W., Ammann, B., and Oldfield, F. (2000). The use of mineral magnetism in the reconstruction of fire history: A case study from Lago di Origlio, Swiss Alps. *Palaeogeogr. Palaeoclimatol. Palaeoecol.* 164, 101–110.

Goldberg, A., Mychajliw, A. M., and Hadly, E. A. (2016). Post-invasion demography of prehistoric humans in South America. *Nature* 532, 232–235.

Hanelt, P., Büttner, R., and Mansfeld, R. (2001). *Mansfeld's Encyclopedia of Agricultural and Horticultural Crops (Except Ornamentals)*. Berlin: Springer.

Higuera, P. E., Brubaker, L. B., Anderson, P. M., Feng, S. H., and Brown, Thomas, A. (2009). Vegetation mediated the impacts of postglacial climate change on fire regimes in the south-central Brooks Range, Alaska. *Ecol. Monogr.* 79, 201–219.

Higuera, P. E., Gavin, D. G., Bartlein, P. J., and Hallett, D. J. (2010). Peak detection in sediment–charcoal records: impacts of alternative data analysis methods on fire-history interpretations. *Int. J. Wildl. Fire* 19, 996. Available at: http://www.publish.csiro.au/?paper=WF09134.

Higuera, P., Peters, M., Brubaker, L., and Gavin, D. (2007). Understanding the origin and analysis of sediment-charcoal records with a simulation model. *Quat. Sci. Rev.* 26, 1790–1809.

Hogg, A. G., Hua, Q., Blackwell, P. G., Niu, M., Buck, C. E., Guilderson, T. P., et al. (2013). SHCal13 Southern Hemisphere calibration, 0–50,000 years cal BP. *Radiocarbon* 55, 1889–1903.

Levis, C., Costa, F. R. C., Bongers, F., Peña-Claros, M., Clement, C. R., Junqueira, A. B., et al. (2017). Persistent effects of pre-Columbian plant domestication on Amazonian forest composition. *Science (80-.).* 355, 925–931.

Maezumi, S. Y., Alves, D., Robinson, M., Gregorio de Souza, J., Levis, C., Barnett, R. L., et al. (2018). The legacy of 4,500 years of polyculture agroforestry in the eastern Amazon. *Nat. Plants*.

Marlon, J. R., Bartlein, P. J., Carcaillet, C., Gavin, D. G., Harrison, S. P., Higuera, P. E., et al. (2008). Climate and human influences on global biomass burning over the past two millennia. *Nat. Geosci.* 1, 697–702.

Nowaczyk, N. R. (2001). "Logging of magnetic susceptibility," in *Tracking environmental change using lake sediments* (Potsdam, Germany: Springer Netherlands), 155–170.

Power, M. J., Marlon, J., Ortiz, N., Bartlein, P. J., Harrison, S. P., Mayle, F. E., et al. (2008). Changes in fire regimes since the Last Glacial Maximum: An assessment based on a global synthesis and analysis of charcoal data. *Clim. Dyn.* 30, 887–907.

R Foundation for Statistical Computing (2014). R Core Development Team, 2014, R: A language and environment for statistical computing.

Ramsey, C. B., and Lee, S. (2013). Recent and planned developments of the program OxCal. *Radiocarbon* 55, 720–730.

Reimer, P. J., Bard, E., Bayliss, A., Beck, J. W., Blackwell, P. G., Bronk Ramsey, C., et al. (2013). IntCal13 and Marine13 radiocarbon age calibration curves 0-50,000 years cal BP. *Radiocarbon* 55, 1869–1887.

Reynolds, R., Belnap, J., Reheis, M., Lamothe, P., and Luiszer, F. (2001). Aeolian dust in Colorado Plateau soils: Nutrient inputs and recent change in source. *Proc. Natl. Acad. Sci.* 98, 7123–7127.

Shennan, S., Downey, S. S., Timpson, A., Edinborough, K., Colledge, S., Kerig, T., et al. (2013). Regional population collapse followed initial agriculture booms in mid-Holocene Europe. *Nat. Commun.* 4.

Stockmarr, J. (1971). Tablets with spores used in absolute pollen analysis. *Pollen et spores*.

Stuiver, M., and Polach, H. A. (1977). Discussion reporting of 14C data. *Radiocarbon* 19, 355–363. doi:DOI: 10.1017/S0033822200003672.

Timpson, A., Colledge, S., Crema, E., Edinborough, K., Kerig, T., Manning, K., et al. (2014). Reconstructing regional population fluctuations in the European Neolithic using radiocarbon dates: a new case-study using an improved method. *J. Archaeol. Sci.* 52, 549–557.

Whitlock, C., and Larsen, C. (2002). "Charcoal as a fire proxy," in *Tracking environmental change using lake sediments* (Springer), 75–97.

Whitney, B. S., Rushton, E. A., Carson, J. F., Iriarte, J., and Mayle, F. E. (2012). An improved methodology for the recovery of Zea mays and other large crop pollen, with implications for environmental archaeology in the Neotropics. *The Holocene* 22, 1087–1096.

2 Supplementary Figures and Tables

2.1 Supplementary Figures

Supplementary Figure S1. Euclidean and Jaccard Distance measures. Solid line indicated non filtered fossil pollen data, dashed line represents filtered pollen taxa with at least 1% abundance and occurring in at least 5 samples.

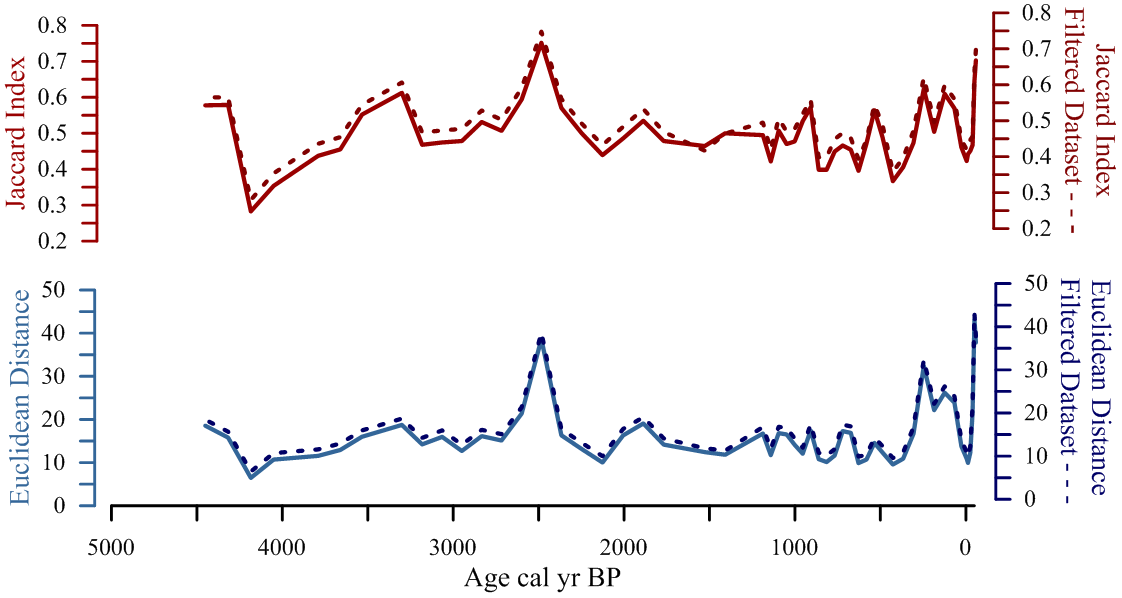

Supplementary Figure 2. Lake Caranã pollen diagram including Pollen Accumulation Rate (PAR), Euclidean Distance and Jaccard similarity index.

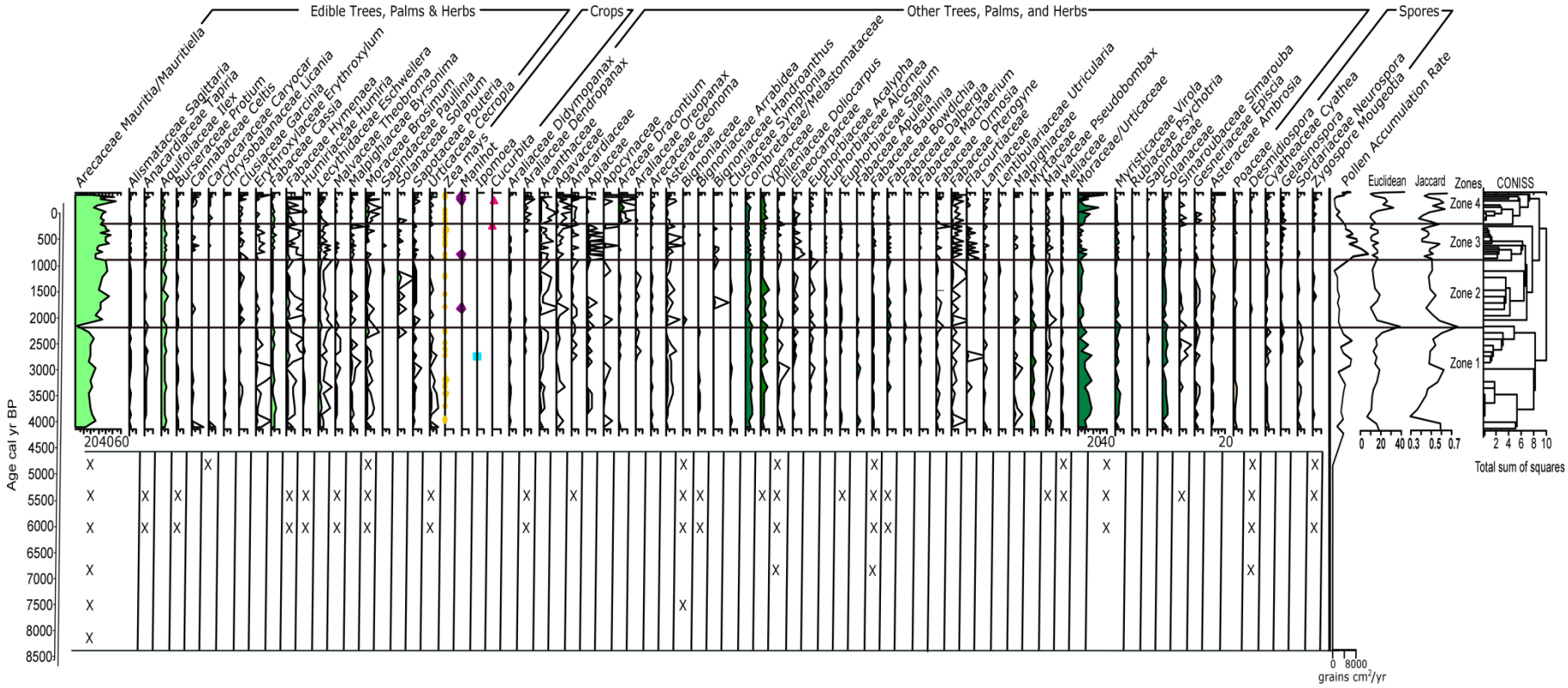

Supplementary Figure 3. Soil photolith profiles from Serra do Maguari archaeological site located on the Belterra Plateau (Maezumi et al., 2018).

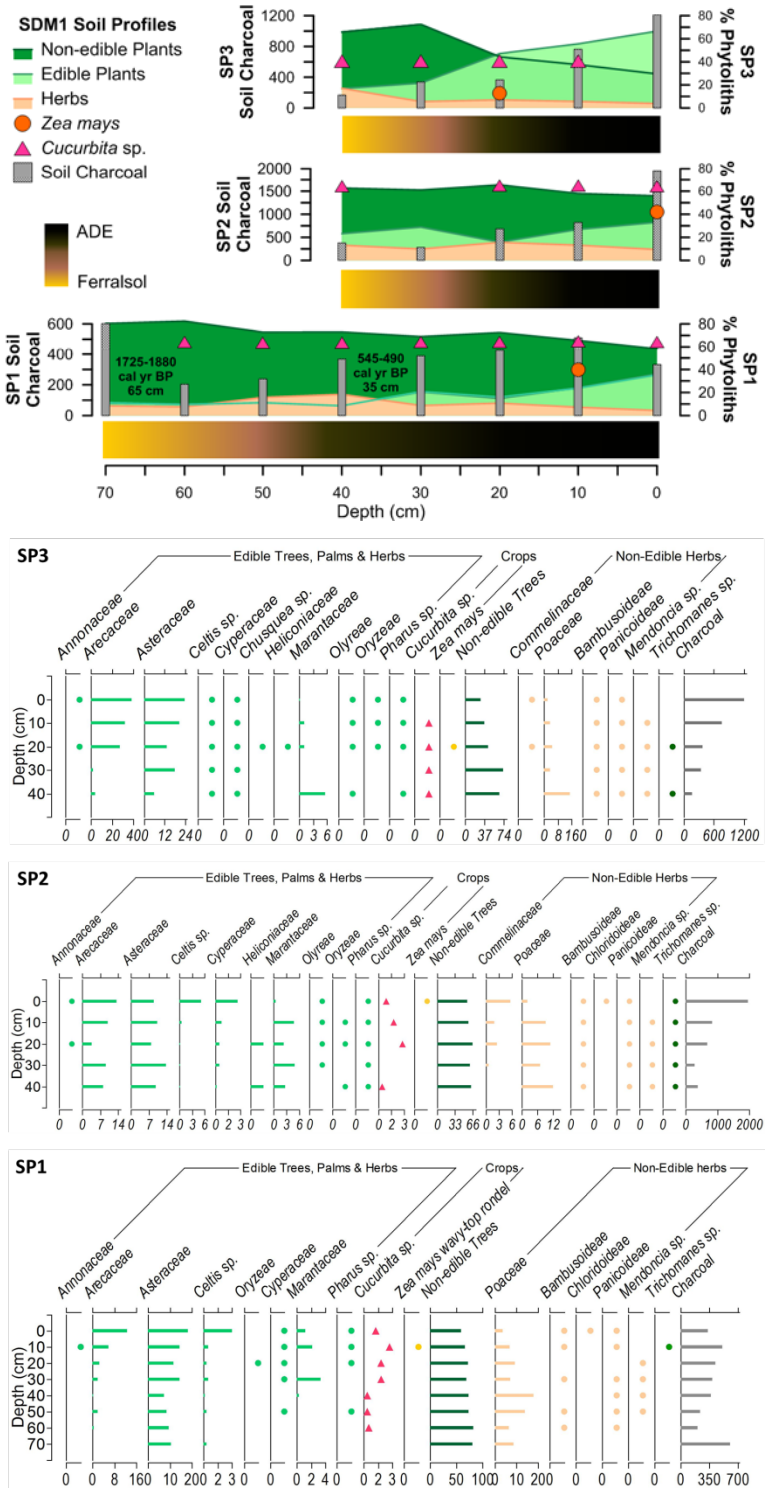

2.1 Supplementary Tables

Method	Depth	**Lab Code**	**^{14}C yrs BP**	Cal. Age B.P. (2σ)
^{14}C	0.35 ±0.005	Beta-433637	520 ±30	517 ±27
^{14}C	0.65 ±0.005	Beta-479517	1870 ±30	1769 ±60

Table 1: *AMS Dates for Serro do Maguari* Archaeological Site